2.4 SEA SURFACE TEMPERATURE PATTERNS ON THE WEST FLORIDA SHELF USING GROWING HIERARCHICAL SELF-ORGANIZING MAPS

Yonggang Liu[1*], Robert H. Weisberg[1] and Ruoying He[2]

1 College of Marine Science, University of South Florida, St. Petersburg, Florida
2 Wood Hole Oceanographic Institution, Woods Hole, Massachusetts

1. INTRODUCTION

The West Florida Shelf (WFS) is a broad, gently sloping continental margin that is influenced by the Gulf of Mexico Loop Current system located seaward of the shelf break (Molinari et al., 1977; Huh et al., 1981; Paluszkiewicz et al., 1983; He and Weisberg, 2003; Weisberg and He, 2003) and by local wind and buoyancy forcing, including the fresh water of the Mississippi River, generally found at mid-shelf in spring and summer (Gilbes et al., 1996; He and Weisberg, 2002). The shelf circulation is dynamically linked to its varying water properties, and particularly to temperature, which exerts a primary control on density. The close relationship between the shelf water temperature variability and the variability of net surface heat flux and ocean circulation are reported in recent studies (He and Weisberg, 2002&2003; Weisberg and He, 2003; Liu and Weisberg, 2004a). Thus, the description of characteristic patterns of the SST variability adds to our understanding of the shelf circulation and air-sea interactions (Weisberg et al., 2004).

1.1 Self-Organizing Map and its Applications in Meteorology and Oceanography

Techniques for pattern detection in large oceanographic data sets are becoming increasingly important as data sets grow in size and complexity. The Self-Organizing Map (SOM), an artificial neural network based on unsupervised learning, is an effective software tool of feature extraction (Kohonen 1982 & 2001). It provides a nonlinear cluster analysis, mapping high-dimensional data onto a (usually) 2D output space while preserving the topological relationships between the input data. As a tool of pattern recognition and classification, the SOM analysis is in widespread use across a number of disciplines (Kaski et al., 1998; Oja et al., 2003). Since its first use in climate research by Hewitson and Crane (1994), extensive applications of the SOM technique have been found in meteorological community (Malmgren, 1999; Cavazos, 1999&2000; Ambroise et al., 2000; Cavazos et al., 2002; Hewitson and Crane, 2002). Recently, the SOM analysis has also been applied in oceanography. For example, Ainsworth (1999) and Ainsworth and Jones (1999) used this method to improve chlorophyll estimates from satellite data. Silulwane et al. (2001) and Richardson et al. (2002) used it to identify characteristic chlorophyll profiles in the ocean, and Hardman-Mountford et al. (2003) applied this method to altimeter data. Ultsch and Röske (2002) used it to predict sea level. The SOM technique was also used to extract SST and wind patterns from satellite data (Richardson et al., 2003; Risien et al., 2004), and to detect ocean current spatial patterns from moored velocity time series (Liu and Weisberg, 2004b).

1.2 Growing Hierarchical Self-Organizing Map

Despite its wide applications, the SOM analysis has its inherent deficiencies. First, it uses a static network architecture w.r.t. the number and arrangement of neural nodes, that have to be defined prior to the start of training. Second, hierarchical relations between the input data are difficult to detect in the map display. To address both issues within one framework, a neural network model of the Growing Hierarchical Self-Organizing Map (GHSOM) was recently introduced (Dittenbach et al., 2002; Rauber et al., 2002; Dittenbach, 2003; Pampalk et al., 2004). The GHSOM is composed of independent SOMs, each of which is allowed to grow in size during the training process until a quality criterion regarding data representation is met. This growth process is further continued to form a layered architecture such that hierarchical relations between input data are further detailed at lower layers of the neural network. To our knowledge, the GHSOM method has not yet been applied to meteorological or oceanographic research.

1.3 SOM and GHSOM MATLAB Toolboxes

Most of the above referenced SOM applications in meteorology and oceanography are based on a software package SOM_PAK 3.1 or earlier versions (Kohonen et al., 1995), written in C language. However, the Mathwork Inc.'s MATLAB has been steadily gaining popularity as the "language of scientific computing". Moreover, MATLAB is much better suited for fast prototyping and customizing than C language, as MATLAB employs a high-level programming language with strong support for graphics and visualization. The SOM Toolbox takes advantage of these strengths and provides an efficient, customizable SOM implementation (Vesanto et al., 2000). The SOM Toolbox utilizes

* *Corresponding author address*: Yonggang Liu, Univ. of South Florida, 140 7th Ave S, St. Petersburg, FL 33701, email: yliu@marine.usf.edu

MATLAB structures and the functions are constructed modularly, making it convenient to tailor the code for specific user needs. The SOM Toolbox version 2.0 can be downloaded at a website of the Helsinki University of Technology, Finland: http://www.cis.hut.fi/projects/somtoolbox/. The GHSOM Toolbox, developed jointly by the University of Aberdeen and Vienna University of Technology, can be downloaded at http://www.oefai.at/~elias/ghsom/.

1.4 Goal of This Paper

A five-year set of daily SST composite maps on the WFS are analyzed using the SOM and the GHSOM Toolboxes. The purposes are two fold: (1) to demonstrate the usefulness of the GHSOM in feature extraction, and (2) to describe the characteristic SST patterns on the WFS and their temporal variations.

Since the GHSOM method is relatively new to the oceanographic community, a brief discussion on the philosophy behind the SOM and GHSOM techniques is given in section 2. The SST data set is described in section 3. Applications of the linear, EOF and the nonlinear, GHSOM methods are described in sections 4 and 5, respectively. The results are discussed in section 6, and the paper is summarized in section 7.

2. MORE ON THE SOM AND GHSOM

In this section, a brief introduction of the SOM and GHSOM methods is given based on work by Kohonen (1982 & 2001), Dittenbach et al. (2002), Dittenbach (2003) and Pampalk et al. (2004). The SOM is a nonlinear, ordered, smooth mapping of high-dimensional input data onto the elements of a regular, low-dimensional (usually 2D) array (Kohonen 1982 & 2001). Fig. 1 gives an illustration of how a SOM works. The SOM consists of a set of i units arranged in a 2D grid with a weight vector $\mathbf{m}_i$ attached to each unit, which may be initialized randomly. Input vectors $\mathbf{x}$ are presented to the SOM and the activation of each unit for the presented input vector is calculated using an activation function. Commonly, it is the Euclidian distance between the weight vector of the unit and the input vector that serves as the activation function. In the next step the weight vector of the unit showing the highest activation (i.e. the smallest Euclidian distance) is selected as the "winner" c_k where

$$c_k = \arg\min_i \left\| \mathbf{x}_k - \mathbf{m}_i \right\| \qquad (1)$$

The weight vector of the winner is moved toward the presented input signal by a certain fraction of the Euclidean distance as indicated by a time-decreasing learning rate α. The learning rate α can be an inverse-time, linear or power function. Thus, this unit's activation will be even higher the next time the same input signal is presented. Moreover, the weight vectors of units in the neighborhood of the winner are also modified according to a spatial-temporal neighborhood function ε. Similar to the learning rate, the neighborhood function ε is time-decreasing. Also, ε decreases spatially away from the winner. There are many types of neighborhood function, and the typical one is Gaussian. The learning rule may be expressed as

$$\mathbf{m}_i(t+1) = \mathbf{m}_i(t) + \alpha(t) \cdot \varepsilon(t) \cdot [\mathbf{x}(t) - \mathbf{m}_i(t)] \qquad (2)$$

where t denotes the current learning iteration and $\mathbf{x}$ represents the currently presented input pattern. This learning procedure leads to a topologically ordered mapping of the presented input data. Similar patterns are mapped onto neighboring regions on the map, while dissimilar patterns further apart.

The GHSOM enhances the capabilities of the basic SOM in two ways. The first is to use an incrementally growing version of the SOM, which does not require the user to directly specify the size of the map beforehand; the second enhancement is the ability to adapt to hierarchical structures in the data (Dittenbach et al., 2002; Rauber et al., 2002; Dittenbach, 2003; Pampalk et al., 2004). Fig. 2 gives a cartoon show of the GHSOM. Prior to the training process a "map" in layer 0 consisting of only one unit is created. This unit's weight vector is initialized as the mean of all input vectors and its mean quantization error (MQE) is computed. The MQE of unit i is computed as

$$MQE_i = \frac{1}{|U_i|} \sum_{k \in U_i} \left\| \mathbf{x}_k - \mathbf{m}_i \right\|, \qquad U_i = \left\{ k \middle| c_k = i \right\}. \qquad (3)$$

Beneath the layer 0 map a new SOM is created with a size of initially 2×2 units. The intention is to increase the map size until all data items are represented well. A mean of all MQE_i is obtained as $\langle MQE \rangle$. The $\langle MQE \rangle$ is then compared to the MQE in the layer above, $\langle MQE \rangle_{above}$. If the following inequality is fulfilled a new row or column of map units are inserted in the SOM,

$$\langle MQE \rangle > \tau_1 \cdot \langle MQE \rangle_{above} \qquad (4)$$

where τ_1 is a user defined parameter. Once the decision is made to insert new units the remaining question is where to do so. In the GHSOM array, the unit i with the largest MQE_i is defined as the *error unit*. Then the most dissimilar adjacent neighbor, i.e., the unit with the largest distance in respect to the model vector, is selected and a new row or column is inserted between these. If the inequality (4) is not satisfied, the next decision to be made is whether some units should be expanded on the next hierarchical level or not. If the data mapped onto one single unit i still has a larger variation, i.e.,

$$MQE_i > \tau_2 \cdot \langle MQE \rangle_{above} \qquad (5)$$

where τ_2 is a user defined parameter, then a new map will be added at a subsequent layer. Generally, the values for τ_1 and τ_2 are chosen such that $1 > \tau_1 >> \tau_2 > 0$. In the GHSOM Toolbox, τ_1 and τ_2 are called "breadth"- and "depth"-controlling parameters, respectively. Generally, the smaller the parameter τ_1, the larger the SOM arrays will be. The smaller the parameter τ_2, the more layers the GHSOM will have in the hierarchy.

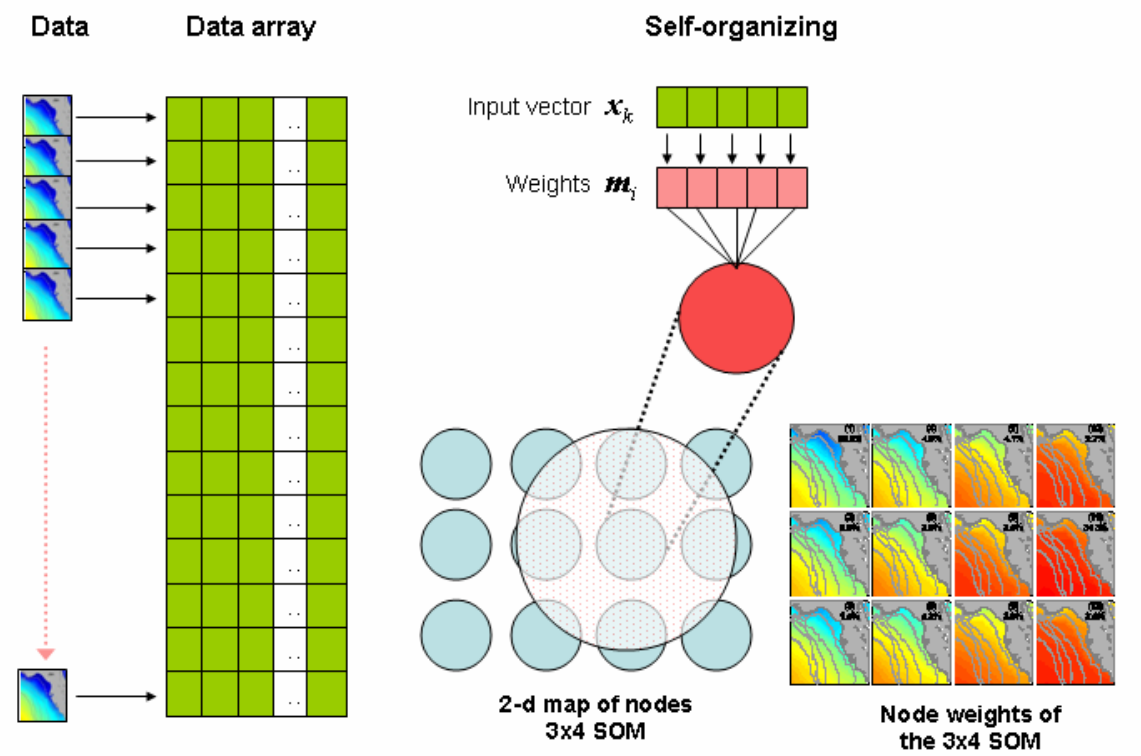

Fig. 1. Illustration of how a SOM works. The data time series are rearranged to form a big 2D data array such that the data at each time step are reshaped to be a row vector. For each time step, the row vector is used to update the weight of the SOM via an unsupervised learning algorithm. This iteration process is called self-organizing. The outcome weight vectors of the SOM nodes are reshaped back to have characteristic data patterns.

3. DATA

A time series of daily SST on the WFS were generated by merging the Advanced Very High Resolution Radiometer SST and the Tropical Rainfall Measuring Mission Microwave Imager SST data via an optimal interpolation scheme (He et al., 2003). We chose the initial five-year period spanning January 1998 through December 2002 for an analysis here. The data domain is shown in Fig. 3, which is a little smaller than that of He et al. (2003), focusing more on the WFS. If the data set is arranged in an *I*×*J* matrix, where *I* and *J* are spatial and temporal dimensions, respectively, then a temporal mean SST pattern is expressed as

$$\overline{T}(x) = \frac{1}{J}\sum_{j=1}^{J} T(x,t_j) \qquad (6)$$

and shown in Fig. 3. The five-year mean pattern shows the warm Loop Current water seaward of the shelf break and the relatively cooler water along the coast near the Florida Big Bend region. The SST gradient points from the southwest to the northeast, with an approximate 30~40° angle deviation from the mean along-isobath direction. This may reflect the combined effects of latitudinal differences in surface heating due to solar radiation and across-shelf differences in water column heating/cooling due to the depth gradient on the shelf.

Two types of SST anomalies are prepared. The first type, $\hat{T}(x,t)$, is obtained by subtracting the temporal mean map from the original data

$$\hat{T}(x,t) = T(x,t) - \overline{T}(x) \qquad (7)$$

By further subtracting a time series of spatial mean values, which is expressed as

$$\overline{\overline{T}}(t) = \frac{1}{I}\sum_{i=1}^{I} \hat{T}(x_i,t)\,, \qquad (8)$$

the second type SST anomaly, $\tilde{T}(x,t)$, is obtained as

$$\tilde{T}(x,t) = T(x,t) - \overline{T}(x) - \overline{\overline{T}}(t) \qquad (9)$$

The spatial mean SST anomaly has higher values in summer and lower values in winter, and the temporal variation is close to a sine function (Fig. 4).

The monthly mean SST patterns, computed over the entire five-year analysis period, show a seasonal variation (Fig. 5). An across-shelf SST gradient is found in all the winter months, but not obvious in the summer months. A spring cold tongue structure that is prominent in April and May is consistent with previous literature (e.g., Weisberg et al., 1996; He and Weisberg, 2002). These SST features will be used to compare with those derived from the linear EOF and nonlinear GHSOM analyses.

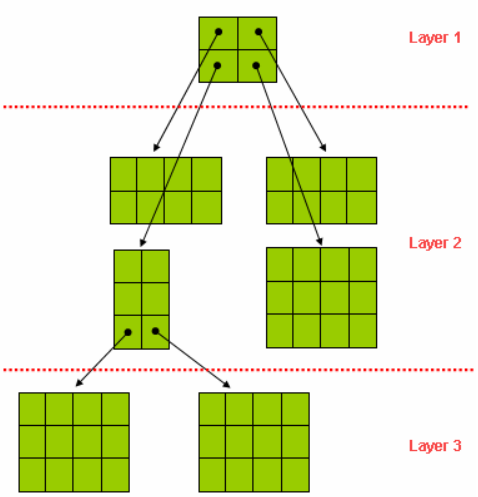

Fig. 2. An example of the Hierarchical structure of the GHSOM. All of the 4 units in the first layer SOM are expanded in the second layer. Only two units in one of the second layer SOMs are further expanded in the third layer.

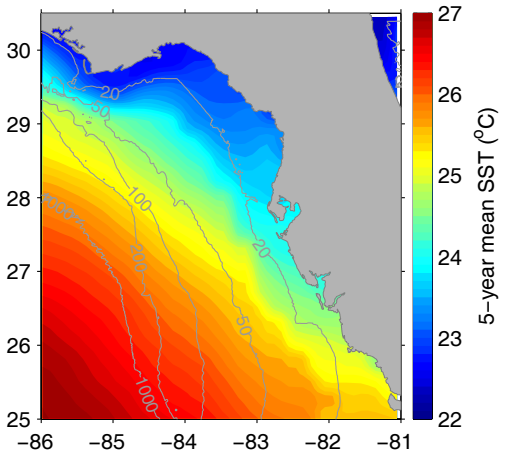

Fig. 3. Record-length mean SST map over the five-year period, 1998-2002, overlaid with 20, 50, 100, 200 and 1000 m isobaths on the WFS.

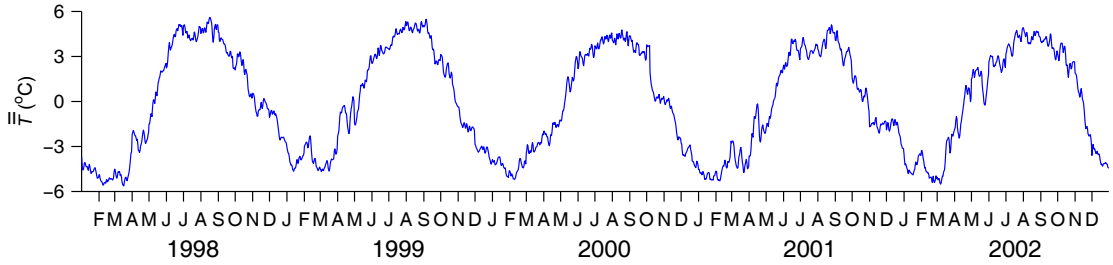

Fig. 4. Time series of the spatial mean SST anomaly on the WFS.

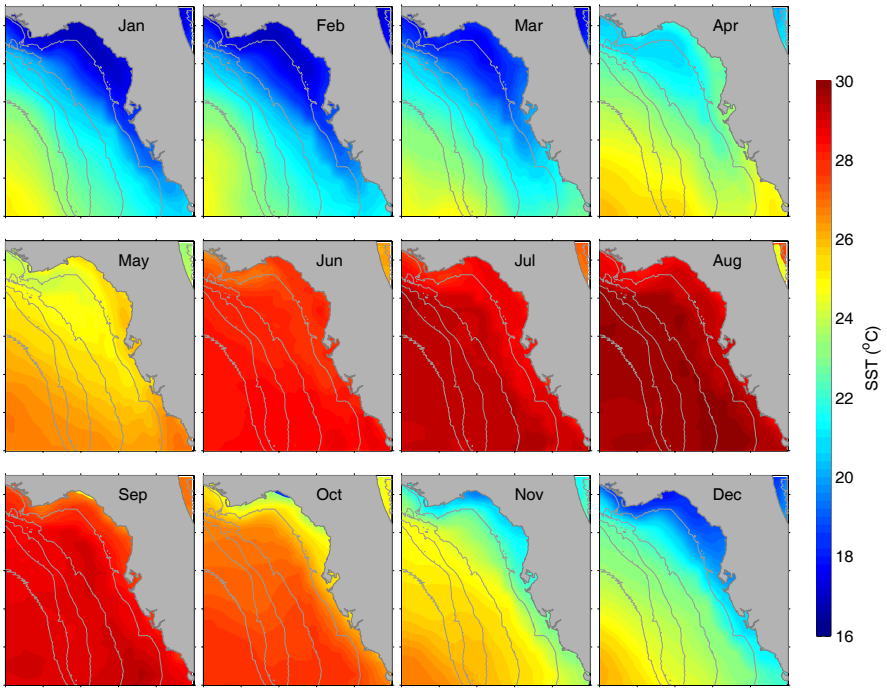

Fig. 5. SST monthly means on the WFS obtained by forming an average for each month over the five-year period, 1998-2002.

4. EOF PATTERNS OF THE SST

Before performing the SOM and GHSOM analyses, we begin with the more established technique of time domain EOF that has wide oceanographic and meteorological applications (e.g., Weare et al., 1976; Richman, 1986; Lagerloef and Bernstein, 1988; Chu et al., 1997a&b; He et al., 2003; Espinosa-Carreon et al., 2004). The EOF is the same as the Principal Component (PC) Analysis (Hotelling, 1933) used in the statistics community. In the combined parlance the PCs are the amplitudes, which are functions of time, of their corresponding spatial eigenfunctions, or EOFs, and the analysis separates the data sets into orthogonal modes. Generally speaking, each mode *n* has an associated variance, a dimensional spatial pattern $F_n(x)$, and a nondimensional time series $\alpha_n(t)$. Thus, the SST anomalies $\hat{T}(x,t)$ may be represented by the EOFs as:

$$\hat{T}(x,t) = \sum_{n=1}^{N} \alpha_n(t) F_n(x) \qquad (10)$$

He et al. (2003) reported EOF results for the first type of SST anomaly defined previously. The first three EOFs of that analysis account for 90.6%, 3.5% and 0.9% of the SST variance, respectively. The dominating first mode represents the seasonal surface heat flux cycle. Note that the strong seasonal variation may hinder our view of other interesting processes. To reduce the impact of the seasonal cycle on the data analysis, the second type SST anomaly data $\tilde{T}(x,t)$ is used, i.e., both the temporal mean map and the spatial mean SST time series are removed from the original SST. Some previous studies removed the seasonal cycle by fitting each time series to annual and semiannual harmonics and subtracting them from the original data (Espinosa-Carreon et al., 2004). In that way, the amplitude of the harmonics being removed may be different from one point to another on a map. We choose to subtract a time series of spatial mean SST simply because the main purpose of the study is to extract the spatial patterns and it is better not to change the relative values on a SST map. Our EOF results are shown in Fig. 6. The first mode, although accounting for a smaller percentage of SST variance (59.6%), has a spatial pattern and temporal variation essentially the same as those in He et al. (2003). It represents the seasonal surface heat flux cycle, i.e., the PC time series has an annual periodicity peaking in summer and winter, and the eigenfunction shows two different regimes, the wide WFS and the deep ocean. This is a consequence of water depth and the buffering effect on the temperature by the warm water advection of the Loop Current. Thus, the Loop Current presents the WFS with a cooling tendency in summer and a warming tendency in winter. The second mode, accounting for 10.8% of the SST variance, reveals a warm/cold tongue pattern on the WFS. The spring cold tongue on the mid WFS is

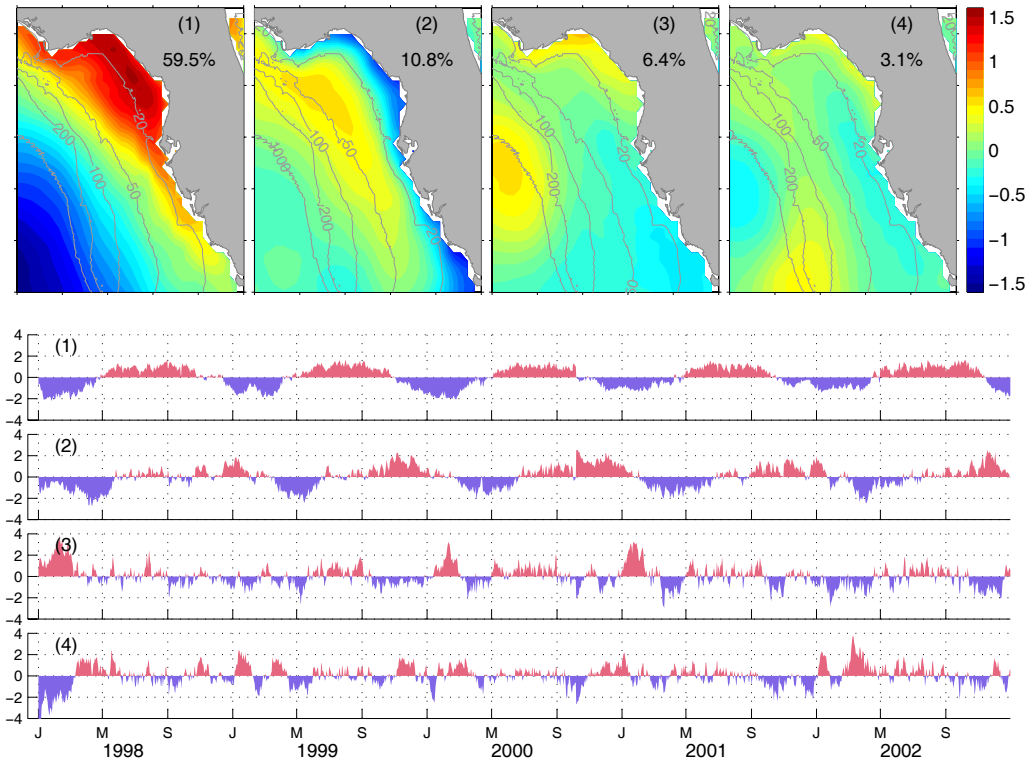

Fig. 6. Eigenfunctions and the associated temporal evolution functions for the first four EOF modes of the SST data. The percent of variance accounted for by each mode is indicated at the upper-right corner of each eigenfunction plot. The tick labels J, M and S on the horizontal axis designate the first days of January, May and September, respectively; same for the following figures.

due to the combined baroclinic and barotropic responses of the WFS circulation to the seasonal surface heat and momentum fluxes as described in previous studies (Weisberg et al., 1996; He and Weisberg, 2002; He et al., 2003). The third mode, accounting for 6.4% of the SST variance, reveals a pattern of the shelf break Loop Current eddy. The fourth mode reveals smaller spatial structures and its PC fluctuations, of higher frequency, are beginning to describe the synoptic scale variability.

5. GHSOM MAPPING OF THE SST

In this section, the GHSOM is performed on the original SST data and the SST anomaly data $\widetilde{T}(x,t)$, respectively.

5.1 GHSOM Analysis of the Original SST Data

The five-year-long daily SST data are used as input to the GHSOM without any preconditioning. In the application of the GHSOM Toolbox, all the parameters are set to the default values except τ_1 and τ_2, the breadth- and depth-controlling parameters. Different (τ_1, τ_2) values are used to test the GHSOM performance (see Table 1). Generally, when smaller (τ_1, τ_2) values are chosen there are more nodes, i.e., larger SOM arrays, in the output. A large SOM array identifies a large number of patterns and reveals more detailed structure within the data, whereas a small SOM array identifies fewer, more generalized patterns. We chose the case of (τ_1=0.6, τ_2=0.06) to analyze simply because the results have two layers and the SOM arrays are large enough to represent characteristic SST features and small enough to be visualized.

Table 1. Performance of the GHSOM with different values of controlling parameters.

τ_1	τ_2	Layer 1 SOM #	Layer 2 SOM #
0.8	0.08	4	4, 0, 0, 4
0.7	0.07	4	6, 4, 0, 4
0.6	0.06	4	12, 6, 0, 10
0.5	0.05	4	30, 15, 18, 55
0.4	0.04	4	64, 40, 48, 119
0.3	0.03	6	132, 120, 96, 0, 144, 140
0.2	0.02	24	0
0.1	0.01	95	0

The layer 1 GHSOM enabled a nonlinear classification of the five-year-long daily SST on the WFS into 4 categories as shown in the 2×2 SOM array in Fig. 7. Each unit explains a particular set of SST characteristics. Unit 1 reveals a typical cold SST pattern (16º < SST < 25ºC); the isotherms are approximately aligned with the isobaths, with the coldest water center around Florida Big Bend region and with the warmest water seaward of shelf break associated with the Loop Current. On the other end of the extremes, unit 4 reveals a warm SST pattern (SST > 28ºC), with no obvious horizontal temperature gradient. Both units 2 and 3 are transitional patterns between the two extremes.

For each of the five-year-long daily SST maps, a best-matching unit (BMU) can be found. The "best" matching is defined to have the smallest weighted distance from the input data. Time series of the BMU number show obvious seasonal fluctuations (Fig. 8). Unit 1 is best-matched in winter, while unit 4 is best-matched in summer. Unit 2 is best-matched in spring and early winter, and unit 3 in early summer and autumn. The cycle of units 1 → 2 → 3 → 4 → 3 → 2 → 1 takes place in one year. In order to quantify the representation of each unit, the frequency of occurrence is computed by summing the hits of that unit and dividing by the total record length. The relative frequency of occurrence of each unit is shown in the upper-right corner of each map in Fig. 7. Unit 1 represents 26.3% of all the SST data, and unit 4 represent 33.7%. Monthly climatology of the frequency of occurrence during the five years is further computed for each unit (Fig. 9). It can be seen that the first pattern mostly appears in January-March, the second pattern in April, November and December, the third pattern in May and October, and the fourth pattern in June-September.

Not all units in the first layer grow to the same depth in the GHSOM hierarchy. Only units 1, 2, and 4 are further expanded in a second layer map. The second layer GHSOM grown from the unit 1 is a category of winter SST patterns. Different features of the coastal cold water and the warm Loop Current water are classified into the 3×4 SOM array (not shown).

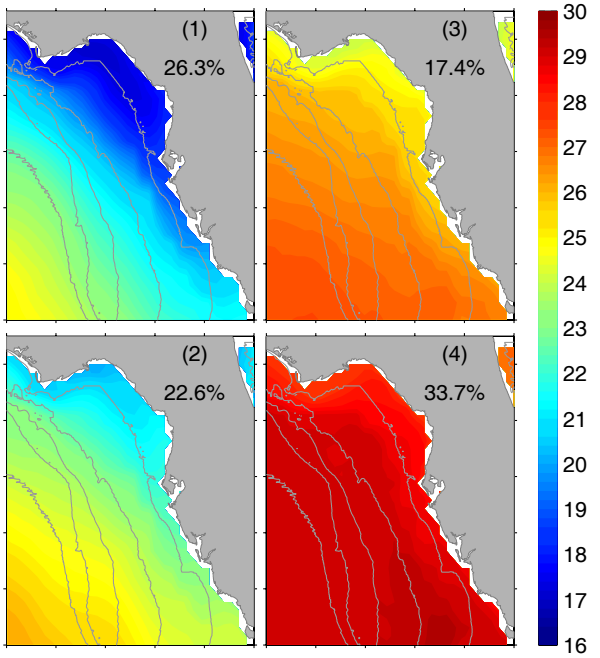

Fig. 7. Layer 1 GHSOM (2×2) of five-year-long daily SST data on the WFS. The frequency of occurrence of each pattern is also shown on each map.

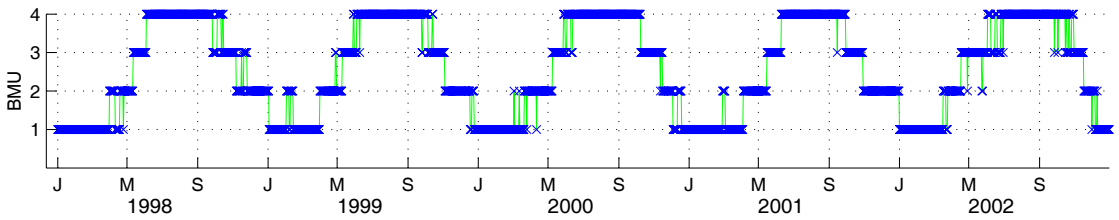

Fig. 8. Temporal evolution of the BMUs. The labels of the vertical axis correspond to the layer 1 GHSOMs in Fig. 7.

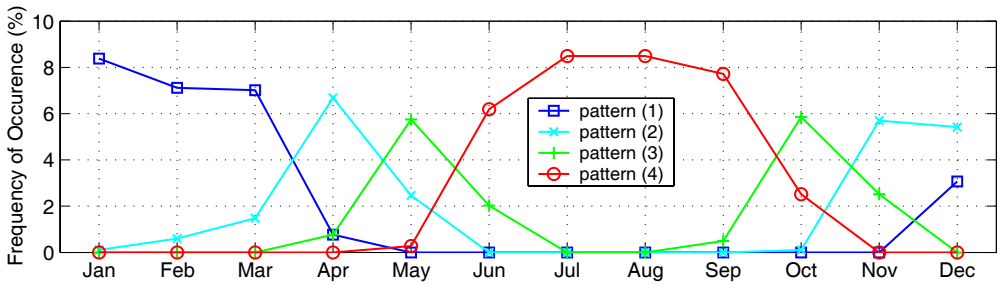

Fig. 9. Frequency of occurrence of the four characteristic patterns as a function of month.

The second layer GHSOM grown from the unit 2 of the first layer GHSOM (GHSOM 2-2) is shown in Fig. 10. This 2×3 array shows a category of spring and early winter SST patterns. Specifically, the upper three units (1, 3, and 5) represent spring patterns, while the lower units (2, 4, and 6) represent early winter patterns; this is distinct in the time series of the BMUs (Fig. 11). The general sequence of the SST variation is unit 1 → 3 → 5 for the spring evolution and unit 6 → 4 → 2 for the early winter evolution. The spring cold tongue structure may be identified in units 3 and 5.

The second layer GHSOM grown from the unit 4 of the first layer GHSOM (GHSOM 2-4, a 2×5 array) shows a category of summer SST patterns (Fig. 12). The peak summer SST patterns are shown in the rhs of the SOM array (units 7~10), while the early and late summer SST patterns are arranged in the lhs (Units 1~6). The evolution of the summer SST patterns from early to late summer stages in each year is illustrated in Fig. 13. The general characteristics of the summer SST is uniformly high temperature. Thus, it is difficult to divide the coastal and the Loop Current waters based on the SST in summer.

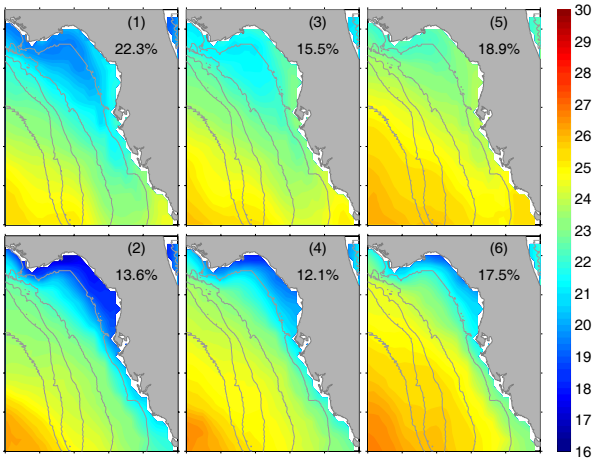

Fig. 10. GHSOM 2-2: Layer 2 SOM under the pattern 2 of the first layer GHSOM. The relative frequency of occurrence of each pattern is shown in the upper-right corner of each map.

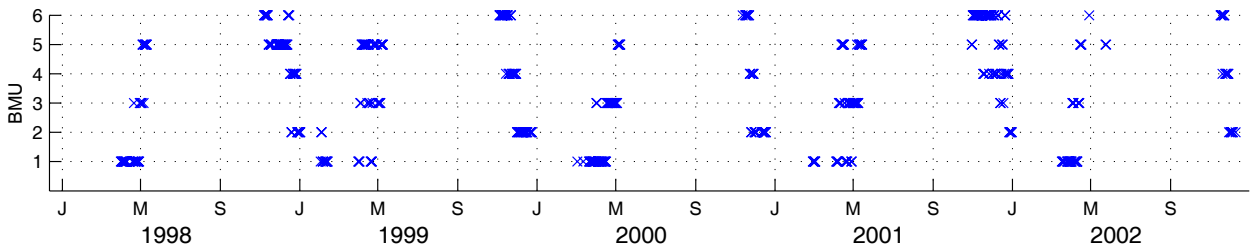

Fig. 11. Temporal evolution of the BMUs for the GHSOM 2-2.

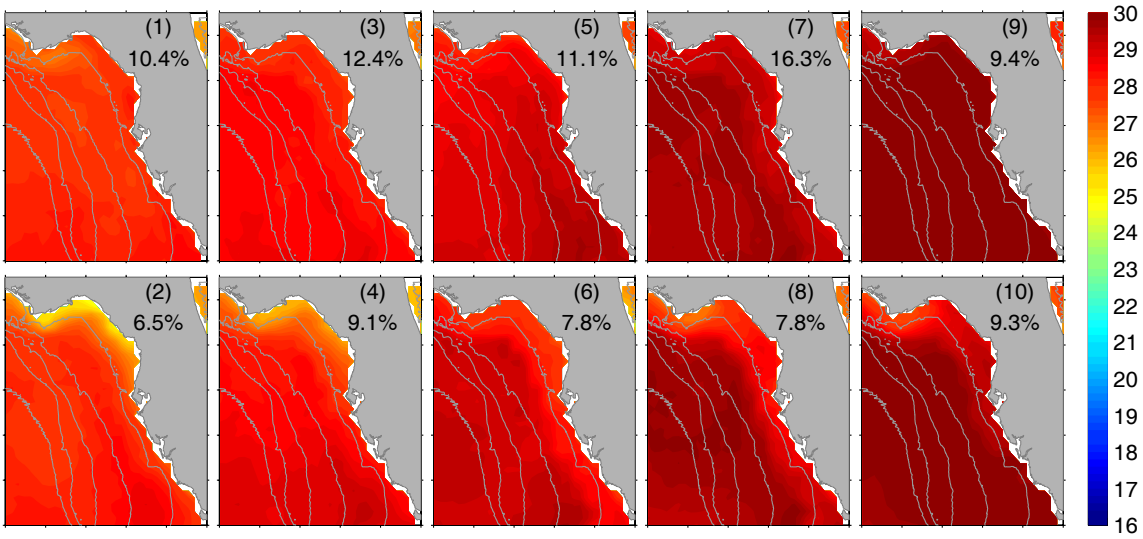

Fig. 12. GHSOM 2-4: Layer 2 SOM under the pattern 4 of the first layer GHSOM. The relative frequency of occurrence of each pattern is shown in the upper-right corner of each map.

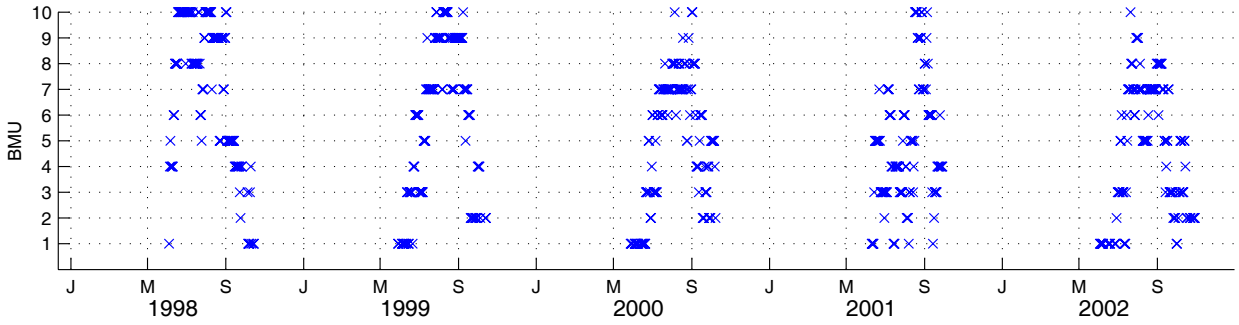

Fig. 13. Temporal evolution of the BMU for the GHSOM 2-4.

5.2 GHSOM Analysis of the SST Anomaly with Both the Temporal Mean Map and Spatial Mean Time Series Removed

The SST anomaly $\widetilde{T}(x,t)$ is used in the GHSOM model. By removing the time series of spatial mean SST, the strong seasonal variation is partially reduced, while the relative spatial structure is not altered, i.e., the horizontal SST gradient is not changed. Similar to that in section 5.1, a set of controlling parameters are used to run the GHSOM model. We choose the result of τ_1=0.8 and τ_2=0.08 to present for the same reason as in section 5.1.

The first layer GHSOM is still a 2×2 array representing four categories of the SST anomaly patterns on the WFS (Fig. 14). Unit 1 reveals a wide warm tongue structure on the shelf, mostly appearing in November as a fall transition (Fig. 15); in contrast, unit 4 reveals a spring cold tongue structure on the shelf (peaking in April). Unit 2 reveals a pattern of coast-ocean contrast in summer (from June through September); on the other hand, unit 3 shows a reversed pattern of the unit 2, prevailing in winter (from January to February). Units 1~4 represent 16.3%, 43.6%, 24.4% and 15.7% of the SST anomaly maps, respectively. Generally, the SST anomaly patterns revealed by the GHSOM may be justified by the first two mode EOFs. Units 2 and 3 resemble the two extremes of the first mode eigenvector with positive and negative weights, respectively; and units 1 and 4 may be ascribed to the second mode EOF with negative and positive weights, respectively. However, the amplitudes of the winter SST anomalies (unit 3) are larger than those of the summer SST anomalies (unit 2); also, the shapes of the cold and warm tongues are different as shown in units 4 and 1, respectively. These asymmetric phenomena are not shown in the EOF results.

All the four units are further expanded at a subsequent layer (not shown). The numbers of the GHSOM units in the second layer are 6, 12, 4 and 6, respectively, for units 1, 2, 3 and 4 in the first layer GHSOM.

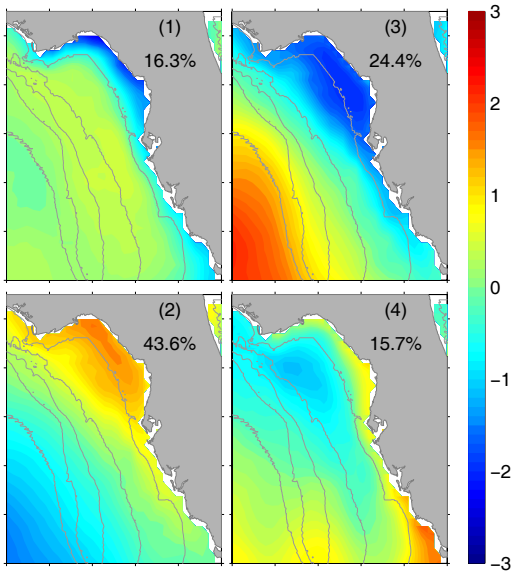

Fig. 14. Layer 1 GHSOM (2×2) of five-year-long daily SST anomalies (τ_1=0.8, τ_2=0.08). The input data is preprocessed by removing both the temporal mean map and a time series of spatial mean values. The relative frequency of occurrence of each pattern is shown in the upper-right corner of each map.

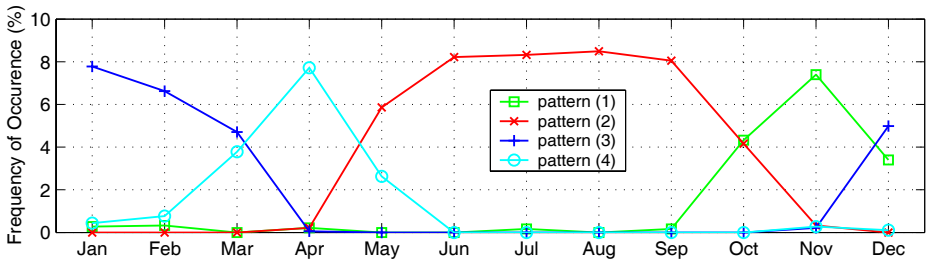

Fig. 15. Frequency of occurrence of the four characteristic maps in Fig. 14 as a function of month.

6. DISCUSSION

As a standard method in data analysis, the EOF can be used conveniently to characterize the dominant spatial patterns of variability as long as the PC time series explains the greatest amount of variance. However, as a linear method it is suboptimal if the system is nonlinear. The SOM can be considered as a nonlinear generalization of the EOF, best preserving the topology rather than the variance of the data. A major strength of the SOM is that the underlying patterns in a data set can be visualized in the same form as the original data. Thus, if input data is SST images, then the outputs are SST patterns, not SST anomaly patterns. This is an advantage over the EOF, in which the temporal mean field has to be removed prior to the analysis. As the SOM output patterns resemble the input format, they are more easily interpreted than output from the EOF. Also, the SOM overcomes the bias of the linear methods, and the SOM patterns may be more realistic than the EOF patterns. As shown in section 5.2, the asymmetric SST anomaly patterns of winter/summer and cold/warm tongues revealed by the SOM array cannot be identified in the EOF patterns. Another advantage of the SOM analysis is that the algorithm is robust in handling missing data, without a priori estimation. Thus, the SOM method can be used to explore incomplete data sets. Moreover, the SOM can be used as data interpolation techniques, estimating missing data from input data that are similar (Hewitson and Crane, 2002).

The major advantages of the GHSOM model over the standard SOM are the following. First, the overall training time is largely reduced since only the necessary number of units are developed to organize the data at a certain degree of detail. Second, the GHSOM uncovers the hierarchical structure of the data, allowing the user to understand and analyze large amount of data in an explorative way. Third, the size of the SOM array does not have to be specified subjectively before hand.

7. SUMMARY

As an extended neural network based on the SOMs, the GHSOMs grow automatically in map size during an

unsupervised training process. Also, the GHSOMs expand in a three-dimensional tree-structure, and represent the inherent hierarchical structure in the data. Each SOM array in the hierarchy explains a particular set of characteristics of the data. This makes the GHSOM analysis an excellent tool for feature extraction and classification.

The GHSOM method is used to extract the characteristic patterns of the SST on the WFS from a time series of daily SST maps that span the five-year interval 1998~2002. Four characteristic SST patterns are extracted in the first layer GHSOM array: characteristic winter and summer SST patterns, and two transitional patterns. Three of them are further expanded in the second layer, yielding more details in the SST pattern evolutions. The results show that a seasonal cycle dominates the SST variability on the shelf. Winter SST pattern is characterized by cold water temperature (16º < SST < 25ºC) with the isotherms approximately aligned with the isobaths and with the coldest water center around Florida Big Bend region and with the warmest water located seaward of shelf break associated with the Loop Current. In contrast, summer SST pattern is characterized by the horizontally uniform, warm water temperature (SST > 28ºC). The spring transition includes a mid shelf cold tongue.

When the GHSOM analysis is performed on the SST anomaly data (with both the temporal mean map and the time series of spatial mean values removed), four characteristic SST anomaly patterns are also obtained in the first layer GHSOM array, representing the SST anomaly patterns in the four seasons. The winter SST anomaly pattern shows the cooling effect of the shelf and warming effect of the Loop Current, while the summer pattern reveals the warming tendency of the shelf and cooling tendency of the Loop Current. The spring pattern shows a mid shelf cold tongue, while the fall pattern shows a warm tongue on the shelf.

It is demonstrated that the GHSOM analysis is more effective in extracting the inherent SST patterns than the widely-used EOF method. The SOM analysis can be considered as a nonlinear generalization of the EOF method, best preserving the topology rather than the variance in the data. The underlying patterns in a data set can be visualized in the SOM array in the same form as the original data, while they can only be expressed in anomaly form in the EOF analysis. Some important features, such as asymmetric SST anomaly patterns of winter/summer and cold/warm tongues, can be revealed by the SOM array but cannot be identified in the EOF patterns. Also, the hierarchical structure in the input data can be extracted by the GHSOM analysis but can not be realized in the EOF technique.

ACKNOWLEDGMENTS

This study was supported by the Office of Naval Research, grant # N00014-98-1-0158 and Task order #:3-12110-10.

REFERENCES

Ainsworth, E. J., 1999: Visualization of ocean colour and temperature from multispectral imagery captured by the Japanese ADEOS satellite. *Journal of Visualization*, **2**, 195–204.

Ainsworth, E. J., & Jones, S. F., 1999: Radiance spectra classification from the ocean color and temperature scanner on ADEOS. *IEEE Trans. Geosci. Remote Sens.*, **37**, 1645–1656.

Ambroise, C., G. Seze, F. Badran, and S. Thiria, 2000: Hierarchical clustering of self-organizing maps for cloud classification. *Neurocomputing.,* **30**, 47–52.

Cavazos, T., 1999: Large-scale circulation anomalies conducive to extreme events and simulation of daily rainfall in northeastern Mexico and southeastern Texas. *J. Climate.,* **12**, 1506–1523.

Cavazos, T., 2000: Using self-organizing maps to investigate extreme climate events: An application to wintertime precipitation in the Balkans. *J. Climate.,* **13**, 1718–1732.

Cavazos, T., A.C. Comrie, and D.M. Liverman, 2002: Intraseasonal variability associated with wet monsoons in Southeast Arizona. *J. Climate*, **15**, 2477-2490.

Chu, P.C., H.C. Tseng, C.P. Chang, and J.M. Chen, 1997a: South China Sea warm pool detected from the Navy's Master Oceanographic Observational Data Set (MOODS). *J. Geophys. Res.*, **102**(C7), 15761-15771 .

Chu, P.C., S.H. Lu, and Y. Chen, 1997b: Temporal and spatial variabilities of the South China Sea surface temperature anomaly. *J. Geophys. Res.*, **102**(C9), 20937-20955.

Dittenbach, M., A. Rauber, and D. Merkl, 2002: Uncovering the hierarchical structure in data using the Growing Hierarchical Self-Organizing Map. *Neurocomputing*, **48**(1-4):199-216

Dittenbach, M., 2003: The growing hierarchical self-organizing map: Uncovering hierarchical structure in data. *Journal of the Austrian Society for Artificial Intelligence*, **22**(3):25-28

Espinosa-Carreon, T. L., P.T. Strub, E. Beier, F. Ocampo-Torres, and G. Gaxiola-Castro, 2004: Seasonal and interannual variability of satellite-derived chlorophyll pigment, surface height, and temperature off Baja California. *J. Geophys. Res.*, **109**(C3), C03039, doi:10.1029/ 2003JC002105.

Gilbes, F., C. Tomas, J. J. Walsh and F. E. Muller-Karger, 1996: An episodic chlorophyll plume on the West Florida Shelf. *Cont. Shelf Res.*, **16**(9), 1201-1224.

Hardman-Mountford N.J., A. J. Richardson , D. C. Boyer , A. Kreiner and H. J. Boyer, 2003: Relating sardine recruitment in the Northern Benguela to satellite-derived sea surface height using a neural network pattern recognition approach. *Progr. in Oceanogr.*, **59**, 241-255.

He, R. and R.H. Weisberg, 2002: West Florida shelf circulation and temperature budget for the 1999 spring transition. *Cont. Shelf Res.*, **22**(5), 719-748.

He, R. and R.H. Weisberg, 2003: West Florida shelf circulation and temperature budget for the 1998 fall transition. *Cont. Shelf Res.*, **23**(8), 777-800.

He, R., R.H. Weisberg, H. Zhang, F. Muller-Karger, and R.W. Helber, 2003: A cloud-free, satellite-derived, sea surface temperature analysis for the West Florida Shelf, *Geophys. Res. Letts.*, **30**, doi:10.1029/2003GL017673.

Hewitson, B. C., & Crane, R. G., 1994: *Neural nets: Applications in Geography*. Kluwer Academic Publishers, 208pp.

Hewitson, B. C., & Crane, R. G., 2002: Self-organizing maps: Applications to synoptic climatology. *Climate Research*, **22**, 13–26.

Hotelling, H., 1933: Analysis of a complex of statistical variables into principal components. *Journal of Educational Psychology*, **24**, 417-441.

Huh O.K., W.J. Wiseman and L.J. Rouse, 1981: Intrusion of Loop Current waters onto the West Florida continental shelf. *J. Geophys. Res.*, **86**(C5), 4186-4192.

Kaski, S., J. Kangas, and T. Kohonen, 1998: Bibliography of Self-Organizing Map (SOM) Papers: 1981-1997. *Neural Computing Surveys*, **1**, 102-350.

Kohonen, T., 1982: Self-organized information of topologically correct features maps. *Biological Cybernetics*, **43**, 59-69.

Kohonen, T., 2001: Self-Organizing Maps. *Springer Series in Information Sciences*, *Vol. 30*, 3rd ed., Springer-Verlag, 501 pp.

Kohonen, J., Hynninen, J. Kangas, and J. Laaksonen, 1995: SOM_PAK, the self-organizing map program, version 3.1. Helsinki University of Technology, Laboratory of Computer and Information Science, Finland, 27 pp.

Lagerloef, G.S.E., and R.L. Bernstein, 1988: Empirical orthogonal function analysis of advanced Very High Resolution Radiometer surface temperature patterns in Santa Barbra Channel, *J. Geophys. Res.*, **93**, 6863-6873.

Liu, Y. and R.H. Weisberg, 2004a: Momentum balance diagnoses for the West Florida Shelf, *Cont. Shelf Res.*, (submitted).

Liu, Y. and R.H. Weisberg, 2004b: West Florida Shelf ocean current spatial patterns using the Self-Organizing Map, *J. Geophys. Res.*, (submitted).

Malmgren, B.A. and A. Winter, 1999: Climate zonation in Puerto Rico based on Principal Components Analysis and an Artificial Neural Network. *J. Climate*, **12**, 977-985.

Molinari, R.L., S. Baig, D.W. Behringer, G.A. Maul, and R. Legeckis, 1977: Winter intrusions of the Loop Current. *Science*, **198**, 505-506.

Oja, M., S. Kaski, and T. Kohonen, 2003: Bibliography of Self-Organizing Map (SOM) papers: 1998-2001 addendum. *Neural Computing Surveys*, **3**, 1-156.

Paluszkiewicz, T., L. P. Atkinson, E. S. Posmentier and C. R. McClain, 1983: Observations of a Loop Current frontal eddy intrusion onto the west Florida Shelf. *J. Geophys. Res.*, **88**(C14), 9639-9651.

Pampalk, E., G. Widmer, and A. Chan, 2004: A new approach to hierarchical clustering and structuring of data with Self-Organizing Maps. *Intelligent Data Analysis Journal*, **8**(2), 131-149.

Rauber, A., D. Merkl, and M. Dittenbach, 2002: The Growing Hierarchical Self-Organizing Map: Exploratory analysis of high-dimensional data. *IEEE Transactions on Neural Networks*, **13**(6):1331-1341.

Richardson, A. J., Pfaff, M. C., Field, J. G., Silulwane, N. F., & Shillington, F. A. (2002). Identifying characteristic chlorophyll a profiles in the coastal domain using an artificial neural network. *Journal of Plankton Research*, **24**, 1289–1303.

Richardson A.J., C. Risien and F. A. Shillington, 2003: Using self-organizing maps to identify patterns in satellite imagery. *Progr. in Oceanogr.*, **59**, 223-239.

Richman, M.B., 1986: Rotation of principal components. *Journal of Climatology*, **6**, 293-235.

Risien, C.M., C.J.C. Reason F.A. Shillington, D.B. Chelton, 2004: Variability in satellite winds over the Benguela upwelling system during 1999–2000. *J. Geophys. Res.*, **109**(C3), C03010, doi:10.1029/2003JC001880.

Silulwane, N. F., A.J. Richardson, F.A. Shillington, and B.A. Mitchell-Innes, 2001: Identification and classification of vertical chlorophyll patterns in the Benguela upwelling system and Angola-Benguela Front using an artificial neural network, In A. I. L. Payne, S. C. Pillar, & R. J. M. Crawford (Eds.), A Decade of Namibian Fisheries Science. *South African Journal of Marine Science*, **23**, 37–51.

Ultsch A. and F. Röske, 2002: Self-organizing feature maps predicting sea levels. *Information Sciences*, **144**, 91-125.

Vesanto, J., J. Himberg, E. Alhoniemi and J. Parhankangas, 2000: SOM Toolbox for Matlab 5, Helsinki University of Technology, Finland.

Weare, B.C., A.R. Navato, and R.E. Newell, Empirical orthogonal analysis of Pacific sea surface temperature. *J. Phys. Oceanogr.*, **6**, 671-678, 1976.

Weisberg, R.H., B. Black and H. Yang, 1996: Seasonal modulation of the west Florida shelf circulation, *Geophys. Res. Lett.*, **23**, 2247-2250.

Weisberg, R.H. and R. He, 2003: Local and deep-ocean forcing contributions to anomalous water properties on the West Florida Shelf. *J. Geophys. Res.,* **108**(C6) 3184, doi:10.1029/2002JC001407.

Weisberg, R.H., R. He, G. Kirkpatrick, F. Muller-Karger and J.J. Walsh, 2004: Coastal ocean circulation influences on remotely sensed optical properties: A West Florida Shelf case study. *Oceanography*, **17**(2), 68-75.